

Galeaspid anatomy and the origin of vertebrate paired appendages

<https://doi.org/10.1038/s41586-022-04897-6>

Received: 20 October 2021

Accepted: 24 May 2022

Published online: 28 September 2022

 Check for updates

Zhikun Gai^{1,2,3}, Qiang Li^{1,4}, Humberto G. Ferrón^{5,6}, Joseph N. Keating⁵, Junqing Wang¹, Philip C. J. Donoghue⁵✉ & Min Zhu^{1,2,3}✉

Paired fins are a major innovation^{1,2} that evolved in the jawed vertebrate lineage after divergence from living jawless vertebrates³. Extinct jawless armoured stem gnathostomes show a diversity of paired body-wall extensions, ranging from skeletal processes to simple flaps⁴. By contrast, osteostracans (a sister group to jawed vertebrates) are interpreted to have the first true paired appendages in a pectoral position, with pelvic appendages evolving later in association with jaws⁵. Here we show, on the basis of articulated remains of *Tujiaaspis vividus* from the Silurian period of China, that galeaspids (a sister group to both osteostracans and jawed vertebrates) possessed three unpaired dorsal fins, an approximately symmetrical hypochordal tail and a pair of continuous, branchial-to-caudal ventrolateral fins. The ventrolateral fins are similar to paired fin flaps in other stem gnathostomes, and specifically to the ventrolateral ridges of cephalaspid osteostracans that also possess differentiated pectoral fins. The ventrolateral fins are compatible with aspects of the fin-fold hypothesis for the origin of vertebrate paired appendages^{6–10}. Galeaspids have a precursor condition to osteostracans and jawed vertebrates in which paired fins arose initially as continuous pectoral–pelvic lateral fins that our computed fluid-dynamics experiments show passively generated lift. Only later in the stem lineage to osteostracans and jawed vertebrates did pectoral fins differentiate anteriorly. This later differentiation was followed by restriction of the remaining field of fin competence to a pelvic position, facilitating active propulsion and steering.

Galeaspids are an extinct group of jawless vertebrates—members of a paraphyletic array of extinct stem gnathostomes that are more closely related to living jawed vertebrates than to lampreys and hagfishes³. As such, they provide key insights into the evolutionary assembly of the gnathostome body plan, including the profound reorganization of the vertebrate skull that occurred before the origin of jaws¹¹. Unfortunately, knowledge of the anatomy of galeaspids has been limited almost exclusively to their headshields; the few incomplete fragments of trunk skeletons that have been discovered^{12–14} provide little insight into the nature of their appendicular skeleton. Therefore, scenarios for the origin and evolution of paired and unpaired fins remain contingent on discovery of the condition in galeaspids. Here we describe an exceptionally preserved and articulated galeaspid from the Silurian period of south China that sheds light on the origin of vertebrate paired appendages.

Systematic palaeontology

Class Galeaspida Tarlo, 1967
Order Eugaleaspidiformes Liu, 1980
Tujiaaspis vividus gen. et sp. nov.

Etymology. The genus name *tujia*, Pinyin for the Tujia people, a minority ethnic group in China, in reference to the two fossil sites

located in Xiangxi Tujia, Miao Autonomous Prefecture, Hunan Province, and Xiushan Tujia, Miao Autonomous County, Chongqing Municipality; *aspis* (Gr.), shield; and species name *vividus* (L.), spirited, full of life.

Holotype. A nearly complete fish accessioned as Institute of Vertebrate Paleontology and Paleoanthropology (IVPP) V26668 (Fig. 1).

Paratype. Two nearly complete and articulated fishes and their counterparts, IVPP V27410 and IVPP V27411 (Fig. 2a).

Locality and horizon. Lianghe village, Yongdong town, Xiushan County, Chongqing Municipality; Kapeng Reservoir, Baojing County, Xiangxi, Hunan Province (Extended Data Fig. 1a); Huixingshao Formation, middle–late Telychian age, Llandovery epoch, Silurian period (about 436 million years old) (Extended Data Fig. 1b).

Differential diagnosis. Small-sized jawless fish up to 70 mm in length with a suite of diagnostic characters of Eugaleaspidiformes, including longitudinal oval median dorsal opening, developed medial dorsal canal and subtriangular headshield with cornual and inner cornual processes. It differs from all known galeaspids in its festooned reticulate sensory canal system with 2–3 subordinate subbranches (autapomorphy); it differs from Shuyuidae, Sinogaleaspidae and Eugaleaspidae in its leaf-shaped inner cornual process; it differs from Tridensaspidae in lacking the rostral process and laterally projecting

¹Key CAS Laboratory of Vertebrate Evolution and Human Origins, Institute of Vertebrate Paleontology and Paleoanthropology, Chinese Academy of Sciences (CAS), Beijing, China. ²CAS Center for Excellence in Life and Paleoenvironment, Beijing, China. ³University of Chinese Academy of Sciences, Beijing, China. ⁴Research Center of Natural History and Culture, Qujing Normal University, Qujing, China. ⁵Bristol Palaeobiology Group, School of Earth Sciences, University of Bristol, Bristol, UK. ⁶Instituto Cavanilles de Biodiversidad i Biologia Evolutiva, Universitat de València, Valencia, Spain. ✉e-mail: phil.donoghue@bristol.ac.uk; zhumin@ivpp.ac.cn

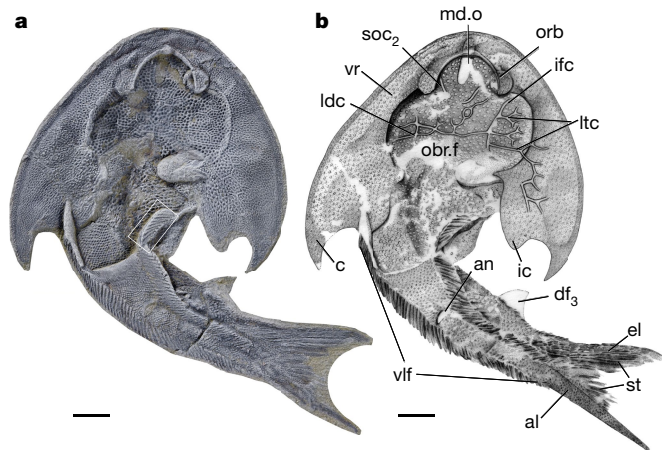


Fig. 1 | Holotype of *T. vividus*. **a, b**, Photograph (a) and interpretative drawing (b) of a complete fish, the holotype, IVPP V26668. The outlined region in a is magnified in Fig. 2e. Scale bars, 4 mm. al, axial lobe; an, anal opening; c, cornual process; df, dorsal fin; el, epichordal lobe; ic, inner cornual process; ifc, infraorbital canal; ldc, lateral dorsal canal; ltc, lateral transverse canal; md.o, median dorsal opening; orb, orbital opening; obr.f, oralbranchial fenestra; soc₂, posterior supraorbital canal; st, strip; vlf, ventrolateral fins; vr, ventral rim.

cornual process. Three unpaired dorsal fins, but the anterior two having joined bases; an approximately symmetrical hypochordal caudal fin, the chordal lobe of which is gently inclined downwards; a pair of pronounced ventrolateral fins that extend continuously from a branchial to a caudal position.

Description

The holotype of *T. vividus* is about 70 mm in length, with a dorsoventrally flattened headshield that comprised about half of its total length and a slightly depressed trunk with a laterally compressed tail (Figs. 1 and 2a,g). The postcranial skeletal anatomy of *T. vividus* is well-preserved in the holotype and paratype (Figs. 1a and 2a). The trunk is elongate and approximately semi-circular in cross-section with slightly convex lateral flanks and an approximately flat ventral surface; it is increasingly laterally compressed in proximity to the tail (Figs. 1 and 2a,g). The trunk inserts into the headshield between the paired inner cornual processes, just posterior to the branchial region, tapering to a fine point caudally (Figs. 1 and 2a,g). The maximum length, width and height of the trunk in the holotype is about 30.5 mm, 13.0 mm and 4.0 mm, respectively (Fig. 1). The trunk is mostly covered in relatively large scales arranged in oblique rows and there are about 16 diamond-shaped scales per mm² (Figs. 1 and 2a,g). Three well-developed erect dorsal fins are observed along the dorsal midline of the body of specimens V27410 and V27411 (df₁₋₃ in Fig. 2a). The anteriormost two dorsal fins are triangular in lateral aspect, with a convex leading edge and a concave rear margin; in specimen V27411 their maximum width is 5.8 mm and 7.6 mm, and their maximum height is 7.5 mm and 3.8 mm (Fig. 2a). They are positioned closer to the headshield than to the tail, just posterior to the inner cornual processes and interconnected such that they may be interpreted as a composite dorsal fin. The third dorsal fin is located at a short distance rostral to the caudal fin and could be the homologue of the anterior part of the epichordal lobe of anaspids, thelodonts and lampreys. It is slightly smaller and more curved, or sickle-shaped, than its two more rostral counterparts, with a maximum width of 5.5 mm and height of 3.6 mm in specimen V27410 (Fig. 2a). The dorsal fins are

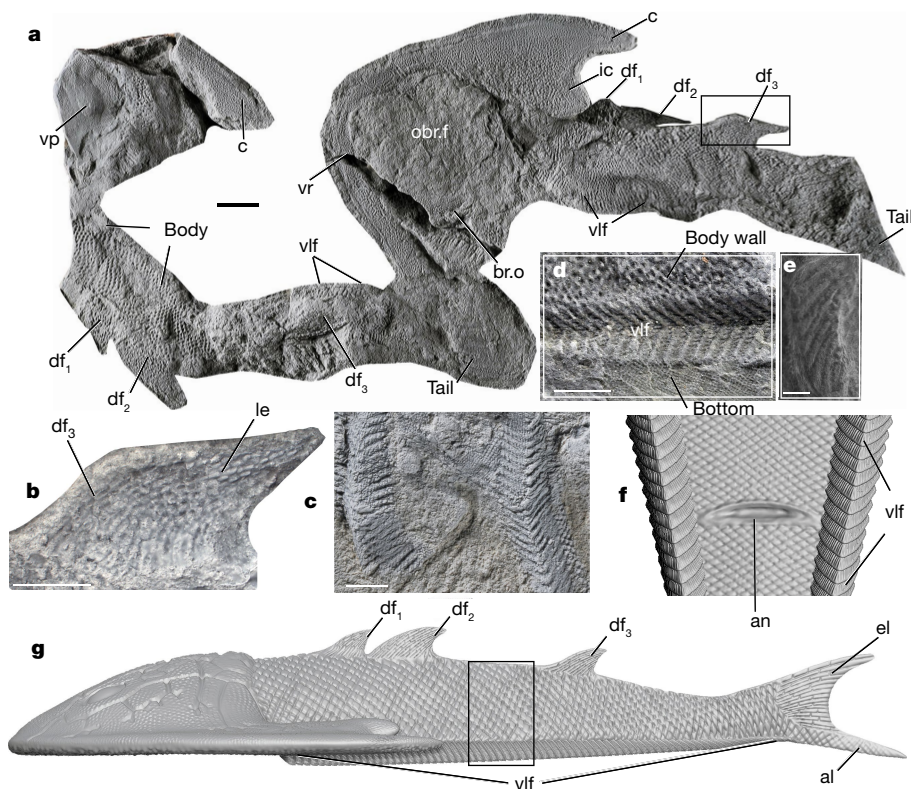


Fig. 2 | The postcranial anatomy of galeaspids. **a**, Photograph of two nearly complete fish preserved together, the paratype of *T. vividus*, IVPP V27410 (right) and IVPP V27411 (left), external mould, in ventral view. **b**, Magnification of the posterior dorsal fin, as outlined in **a**, in lateral view. **c–f**, Magnification of a pair of pronounced ventrolateral fins. **c**, Magnification of specimen IVPP V26669, as outlined in Extended Data Fig. 3b, in ventral view.

d, Magnification of specimen IVPP V27412, in dorsal view. **e**, Scanning electron microscopy image of the holotype IVPP V26668, as outlined in Fig. 1a. **f**, Magnification of the region outlined in **g**, in ventral view. **g**, Virtual three-dimensional reconstruction, in lateral view. br.o, branchial opening; le, lepidotrich-like scale; vp, ventral plate; other abbreviations as in Fig. 1. Scale bars, 4 mm (a), 2 mm (c and d) and 1 mm (b and e).

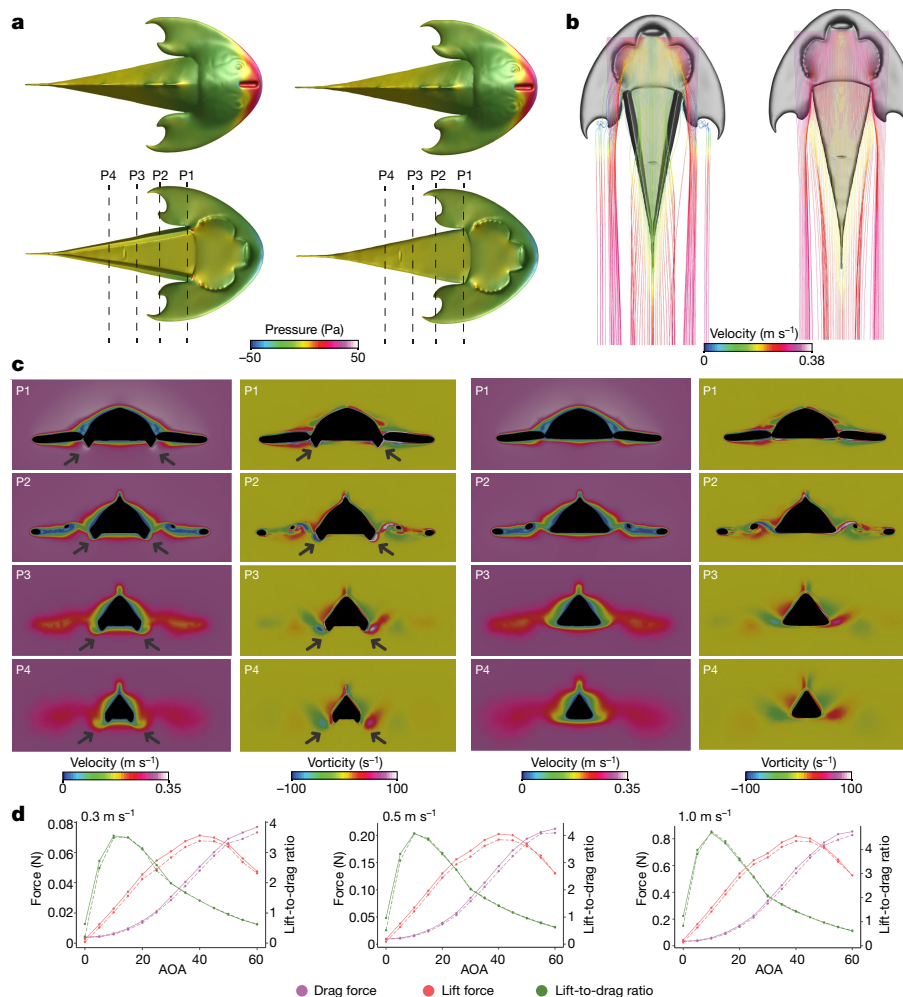


Fig. 3 | Results of CFD simulations. **a, b**, Surface-pressure distribution (**a**) and pathlines patterns of flow along the ventral surface of the body (coloured according to velocity) (**b**) in the models of *Tujiaaspis* with and without ventrolateral ridges (left and right, respectively). **c**, Cross-sectional planes (P1–P4) show the variation in velocity magnitude and Z-vorticity patterns along the models of *Tujiaaspis* with and without ventrolateral ridges (left and right,

respectively). Arrows indicate the position of the ventrolateral fins and the flow disturbances caused by them. These results correspond to simulations at an angle of attack of 0° with an inlet velocity of 0.3 m s^{-1} . **d**, Values of drag and lift forces and the lift-to-drag ratio of CFD simulations at different angles of attack (AOA) and inlet velocities. Data of the models of *Tujiaaspis* with and without ventrolateral ridges are represented as continuous and dashed lines, respectively.

covered in scales organized in a lepidotrich-like linear arrangement (Fig. 2a,b). Elongate dermal tubercles are observed in the posterior part of the third dorsal fin (Fig. 2b). The three dorsal fins do not vary greatly in size, and probably were not very flexible in life.

The caudal fin of *T. vividus* is approximately symmetrical and distinctly hypocercal with a slightly posteroventrally directed axial lobe and a large dorsal epichordal lobe. The axial lobe is very long and tapers to a fine point at its posterior end (Figs. 1 and 2g). Faint traces of the emarginate posterior margin of the epichordal lobe in paratype IVPP V27411 indicates that *T. vividus* probably possessed a slightly forked tail with more than six intermediate, narrower strips composed of radiating ray-like rows of very small scales as in thelodonts and heterostracans (Extended Data Fig. 2b–e). Their precise anatomy remains to be resolved; gaps between the strips of scales could well have been bridged by an unscaled fin web. The ventral surface of the trunk is flat and covered in numerous minute scales (around 49 per mm^2) (Figs. 1 and 2d) that are much smaller than those covering the body dorsally and laterally (Fig. 2d). A small oval orifice preserved in the midline of the abdominal area at about half of the body length is probably the anal opening (cloaca), but no anal fin is observed posterior to the anus (Figs. 1 and 2f).

Perhaps the most unexpected feature of the postcranial anatomy of galeaspid is a pair of pronounced ventrolateral fins that extend

continuously from a branchial to a caudal position, effectively bifurcating from the ventral lobe of the caudal fin. The paired ventrolateral fins are composed of numerous V-shaped skeletal units and covered in elongate, parallel scales (Figs. 1 and 2c–g and Extended Data Fig. 3). These paired fins are similar to the discontinuous pectoral and pelvic fin flaps of thelodonts⁴ and the continuous paired ventrolateral fins of anaspids^{15–18}. They are also morphologically and topologically comparable to the ventrolateral ridges of cephalaspid osteostracans^{19–21}, which, in addition, have differentiated pectoral fins.

To constrain the functional interpretation of the paired ventrolateral fins in *T. vividus*, we subjected virtual models of *T. vividus* with and without these anatomical units (Fig. 3) to experimental analysis using computed fluid dynamics (CFD). Our experiments estimate drag and lift forces as the flow of water over the body is simulated under varying attitudes to the current (angles of attack). The highest pressures exerted on the body occur on the dorsal surface of the snout and the leading edges of the dorsal fins; the lowest pressures occurred on the ventral part of the snout and the most posterior area of the median dorsal opening (Fig. 3a). The presence of the ventrolateral fins in the model has a notable impact, the fins experienced high pressures at the rostral extremity, which directly faced the flow of water. These anatomical structures disrupt the trajectory and velocity of flow, directing the

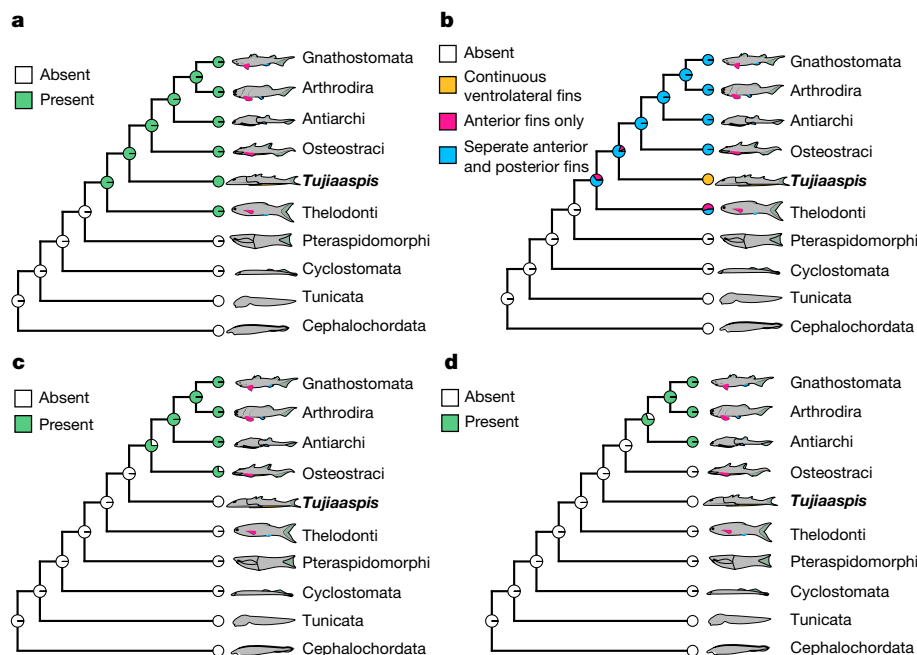


Fig. 4 | Ancestral-state estimation analysis for the evolution of paired appendages in vertebrates. Summary of the results of analyses based on 55 living and extinct chordate taxa, conducted under likelihood and parsimony optimization; the full results are shown in Supplementary Data 4. The phylogenetic framework is based on refs. ^{24,25}. The pie charts on the internal

nodes of the tree reflect the inferred probability of an ancestral character state. **a**, Paired ventrolateral body-wall extensions. **b**, Topological extent of paired flexible ventrolateral fins. **c**, Pectoral appendicular endoskeleton and girdle. **d**, Pelvic appendicular endoskeleton and girdle.

current over the ventral surface of the body (Fig. 3b), slowing down the flow around them and generating stronger vortical structures on their external face (Fig. 3c). In both models, drag and lift forces increase with the angle of attack, but the latter decreases abruptly in all simulations above 40° (that is, stall) (Fig. 3d). Until this point, lift increases with a higher rate and reaches a higher maximum in the model with the ventrolateral fins (Fig. 3d and Extended Data Fig. 4). The model with ventrolateral fins always shows higher lift for equivalent angles of attack and is sufficient to counteract body weight in all scenarios except when positioned at 0°, considering an inlet velocity of 0.3 m s⁻¹ (Supplementary Data 1). This translates to a higher swimming efficiency (lift-to-drag ratio) for the model with the ventrolateral fins at low angles of attack (Fig. 3d), compatible with their interpretation as adaptations for passively generating lift.

The results of our CFD experiments also suggest that, irrespective of a debate regarding their homology^{4,5,22,23}, the prevalence of diverse paired body-wall extensions in jawless stem gnathostomes reflects widespread adaptation to passively generating lift before the origin of muscularized paired fins. In particular, we draw comparison to the morphologically and topologically comparable ventrolateral body-wall extensions in the trunk of cephalaspid osteostracans that are also continuous with the ventral lobe of the caudal fin from which they effectively bifurcate^{19–21}. This structural and topological similarity, combined with the sister relationship between galeaspid and osteostracans plus jawed vertebrates^{24,25} suggests that these structures are a shared characteristic retained in galeaspid and osteostracans, but lost in jawed vertebrates. The ventrolateral body-wall extensions do not extend to the branchial region in cephalaspid, nor do they overlap topologically with the paired pectoral fins. Thus, the acquisition of pectoral fins in osteostracans and jawed vertebrates may reflect division of a broader zone of fin competence into pectoral and post-pectoral domains, retaining the benefits of passive lift facilitated by the ventrolateral fins while also actively generating propulsion and steering through muscularized pectoral fins. The origin of paired pelvic fins in jawed vertebrates may be interpreted as a further caudad

restriction of fin development in this zone of fin competence, representing a permanent shift towards active propulsion associated with the feeding ecology of jawed vertebrates, as long hypothesized by the ‘new head’ hypothesis^{26,27}.

The phylogenetic interpretation of pectoral paired appendages evolving before their pelvic counterparts has imposed considerable constraints on models of their developmental evolution^{1,5,22,28–31}. This constraint may now be relaxed if distinct paired fins are instead interpreted to have emerged phylogenetically from a broader rostro-caudal zone of fin competence that we can now extend from a shared feature of crown gnathostomes³² to a shared primitive character that extends deep into the gnathostome stem lineage. Nevertheless, the emergence of regionalized monobasal fins from ancestors with continuous ventrolateral fins occurred, as found in osteostracans, in the same order of pectoral before pelvic fins. This is similar to, but distinct from the lateral fin-fold hypothesis^{6–10}, which is problematic for a number of reasons^{5,10,33}, albeit especially in regard to its prediction that the pectoral and pelvic fins arose, complete with radials, simultaneously from an ancestrally continuous fin fold. Indeed, the lack of endoskeletal fin elements in fossils of early vertebrates has made the identification of fin homologues and testing of this hypothesis challenging³⁴. However, the absence of endoskeletal elements may not be an artefact of preservation as the results of our CFD experiments are compatible with the view that these structures evolved, initially, to passively generate lift and required no articulation. Only after fin regionalization in co-option for propulsion (such as the monobasal fins of osteostracans and placoderms) did a supporting endoskeleton evolve.

Nevertheless, the available evidence is compatible with the hypothesis that paired fins derived ultimately from heterotopic expression of fin competence that must have originated in unpaired fins because those evolved first. Both paired and unpaired fins have common features in their development, including expression domains of transcription factors (*Hox* and *Tbx*), cell-signalling molecules (*Shh* and *Fgf*) and enhancers (ZRS and sZRS)^{32,35–40}. Caudal extension of the ventrolateral

fins in galeaspid and osteostracans, such that they are continuous with the caudal fin, may be important in supporting the view that this was achieved through bifurcation of an ancestrally ventral midline zone of fin competence⁴¹. In any case, our insights into the postcranial anatomy of galeaspid allow us to constrain uncertainty over the intermediate sequence of evolutionary steps through which the monobasal paired fins of living jawed vertebrates evolved from the unpaired fins of the ancestral vertebrate^{31,32}.

Ancestral-state estimation using parsimony and likelihood optimization under alternative topologies of stem-gnathostome interrelations^{24,25} suggests that paired ventrolateral body-wall extensions, as well as flexible paired fins, evolved early in the gnathostome stem lineage, before the divergence of osteostracans and jawed vertebrates (Fig. 4a). In contrast to the lateral fin-fold hypothesis, our results suggest that paired body-wall extensions were separated into pectoral and pelvic regions from the beginning, although this body plan was modified independently in numerous stem-gnathostome lineages, including galeaspid (Fig. 4b). This finding suggests that pectoral and pelvic regionalization through the co-option of existing regulatory domains^{38,42} may have started early in gnathostome evolution. By contrast, appendicular girdles and their associated endoskeletons evolved late in the gnathostome stem lineage. Of these, the pectoral region appeared first, before the divergence of jawed vertebrates (Fig. 4c,d). The pelvic fin evolved subsequently through caudal diminution of the ventrolateral fin, laying the foundation for the disparity of fins and their derivatives that characterize gnathostome biodiversity.

Online content

Any methods, additional references, Nature Research reporting summaries, source data, extended data, supplementary information, acknowledgements, peer review information; details of author contributions and competing interests; and statements of data and code availability are available at <https://doi.org/10.1038/s41586-022-04897-6>.

- Larouche, O., Zelditch, M. L. & Cloutier, R. Fin modules: an evolutionary perspective on appendage disparity in basal vertebrates. *BMC Biol.* **15**, 32 (2017).
- Tulenko, F. J. et al. Body wall development in lamprey and a new perspective on the origin of vertebrate paired fins. *Proc. Natl Acad. Sci. USA* **110**, 11899–11904 (2013).
- Donoghue, P. C. J. & Keating, J. N. Early vertebrate evolution. *Palaeontology* **57**, 879–893 (2014).
- Wilson, M. V. H., Hanke, G. F. & Märss, T. In *Major Transitions in Vertebrate Evolution* (eds Anderson, J. S. & Sues, H.-D.) 122–149 (Indiana Univ. Press, 2007).
- Coates, M. I. The origin of vertebrate limbs. *Development* **1994**, 169–180 (1994).
- Mivart, S. G. Notes on the fins of elasmobranchs, with considerations on the nature and homologues of vertebrate limbs. *Trans. Zool. Soc. Lond.* **10**, 439–484 (1879).
- Thacher, J. K. *Median and Paired Fins: A Contribution to the History of Vertebrate Limbs* Vol. 3 (Connecticut Academy of Arts and Sciences, 1877).
- Balfour, F. M. On the development of the skeleton of the paired fins of Elasmobranchii, considered in relation to its bearings on the nature of the limbs of the vertebrata. *Proc. Zool. Soc. Lond.* **49**, 656–670 (1881).
- Goodrich, E. S. Notes on the development, structure, and origin of the median and paired fins of fish. *Q. J. Microsc. Sci.* **50**, 333–376 (1906).
- Westoll, T. S. (ed.) in *Studies on Fossil Vertebrates* 180–211 (Athlone, 1958).
- Gai, Z. K., Donoghue, P. C. J., Zhu, M., Janvier, P. & Stampanoni, M. Fossil jawless fish from China foreshadows early jawed vertebrate anatomy. *Nature* **476**, 324–327 (2011).

- Liu, Y. H. Lower Devonian agnathans of Yunnan and Sichuan. *Vert. Palasiat.* **13**, 202–216 (1975).
- Pan, J. *New Galeaspid (Agnatha) from the Silurian and Devonian of China* (Geological Publishing House, 1992).
- Pan, J. & Chen, L. Z. Geraspididae, a new family of Polybranchiaspidida (Agnatha) from Silurian of northern Anhui. *Vert. Palasiat.* **31**, 225–230 (1993).
- Stensio, E. A. A new anaspid from the Upper Devonian of Scaumenac Bay in Canada, with remarks on other anaspids. *K. Svenska Vet. Akad. Handl.* **18**, 1–25 (1939).
- Ritchie, A. New light on the morphology of the Norwegian Anaspida. *Skr. Norske Vidensk. Akad. Oslo* **14**, 1–35 (1964).
- Sansom, R. S., Freedman, K., Gabbott, S. E., Aldridge, R. J. & Purnell, M. A. Taphonomy and affinity of an enigmatic Silurian vertebrate, *Jamoytius kerwoodi* White. *Palaeontology* **53**, 1393–1409 (2010).
- Sansom, R. S., Gabbott, S. E. & Purnell, M. A. Unusual anal fin in a Devonian jawless vertebrate reveals complex origins of paired appendages. *Biol. Lett.* **9**, 20130002 (2013).
- Stensio, E. A. *The Cephalaspids of Great Britain* (British Museum, 1932).
- Heintz, A. Cephalaspida from Downtonian of Norway. *Skr. Norske Vidensk. Akad. Oslo* **1939**, 1–119 (1939).
- Ritchie, A. *Ateleaspis tessellata* Traquair, a non-cornuate cephalaspid from the Upper Silurian of Scotland. *Zool. J. Linn. Soc.* **47**, 69–81 (1967).
- Coates, M. I. in *Developmental Patterning of the Vertebrate Limb* (eds Hinchliffe, J. et al.) 325–337 (Plenum, 1991).
- Larouche, O., Zelditch, M. L. & Cloutier, R. A critical appraisal of appendage disparity and homology in fishes. *Fish Fish.* **20**, 1138–1175 (2019).
- Keating, J. N. & Donoghue, P. C. J. Histology and affinity of anaspids, and the early evolution of the vertebrate dermal skeleton. *Proc. R. Soc. B* **283**, 20152917 (2016).
- Miyashita, T., Gess, R. W., Tietjen, K. & Coates, M. I. Non-ammocoete larvae of Palaeozoic stem lampreys. *Nature* **591**, 408–412 (2021).
- Gans, C. & Northcutt, R. G. Neural crest and the origin of the vertebrates: a new head. *Science* **220**, 268–274 (1983).
- Northcutt, R. G. & Gans, C. The genesis of neural crest and epidermal placodes: a reinterpretation of vertebrate origins. *Q. Rev. Biol.* **58**, 1–28 (1983).
- Coates, M. *Hox* genes, fin folds and symmetry. *Nature* **364**, 195–196 (1993).
- Coates, M. I. The evolution of paired fins. *Theory Biosci.* **122**, 266–287 (2003).
- Shubin, N., Tabin, C. & Carroll, S. Fossils, genes and the evolution of animal limbs. *Nature* **388**, 639–648 (1997).
- Pieretti, J. et al. Organogenesis in deep time: a problem in genomics, development, and paleontology. *Proc. Natl Acad. Sci. USA* **112**, 4871–4876 (2015).
- Yonei-Tamura, S. et al. Competent stripes for diverse positions of limbs/fins in gnathostome embryos. *Evol. Dev.* **10**, 737–745 (2008).
- Romer, A. S. Vertebrate evolution. *Copeia* **1962**, 223–227 (1962).
- Johanson, Z. Evolution of paired fins and the lateral somitic frontier. *J. Exp. Zool.* **314B**, 347–352 (2010).
- Sordino, P., van der Hoeven, F. & Duboule, D. *Hox* gene expression in teleost fins and the origin of vertebrate digits. *Nature* **375**, 678–681 (1995).
- Neumann, C. J., Grandel, H., Gaffield, W., Schulte-Merker, S. & Nüsslein-Volhard, C. Transient establishment of anteroposterior polarity in the zebrafish pectoral fin bud in the absence of sonic hedgehog activity. *Development* **126**, 4817–4826 (1999).
- Ahn, D. G., Kourakis, M. J., Rohde, L. A., Silver, L. M. & Ho, R. K. T-box gene *tbx5* is essential for formation of the pectoral limb bud. *Nature* **417**, 754–758 (2002).
- Freitas, R., Zhang, G. J. & Cohn, M. J. Evidence that mechanisms of fin development evolved in the midline of early vertebrates. *Nature* **442**, 1033–1037 (2006).
- Dahn, R. D., Davis, M. C., Pappano, W. N. & Shubin, N. H. Sonic hedgehog function in chondrichthyan fins and the evolution of appendage patterning. *Nature* **445**, 311–314 (2007).
- Letelier, J. et al. A conserved *Shh cis*-regulatory module highlights a common developmental origin of unpaired and paired fins. *Nat. Genet.* **50**, 504–509 (2018).
- Abe, G. & Ota, K. G. Evolutionary developmental transition from median to paired morphology of vertebrate fins: perspectives from twin-tail goldfish. *Dev. Biol.* **427**, 251–257 (2017).
- Freitas, R., Gomez-Skarmeta, J. L. & Rodrigues, P. N. New frontiers in the evolution of fin development. *J. Exp. Zool.* **322**, 540–552 (2014).

Publisher's note Springer Nature remains neutral with regard to jurisdictional claims in published maps and institutional affiliations.

Springer Nature or its licensor holds exclusive rights to this article under a publishing agreement with the author(s) or other rightsholder(s); author self-archiving of the accepted manuscript version of this article is solely governed by the terms of such publishing agreement and applicable law.

© The Author(s), under exclusive licence to Springer Nature Limited 2022

Methods

Specimens and provenance

The specimens of *T. vividus* described in this study were collected from the upper part of the Huixingshao Formation (middle–late Telychian age of the Llandovery epoch, Silurian period) at two fossil sites: the Kapeng Reservoir of Baojing county (Xiangxi Tujia and Miao Autonomous Prefecture) and the Xiushan area of Chongqing municipality (Xiushan Tujia and Miao Autonomous County) (Extended Data Fig. 1a). The Silurian marine strata in western Hunan and eastern Chongqing include the Lungmachi, Hsiaohopa, Rongxi, Xiushan, Huixingshao and Xiaoxi formations in ascending chronological order^{43–46} (Extended Data Fig. 1b). Three fish-bearing strata, including the Rongxi, Huixingshao and Xiaoxi formations, are recognized in this region and correlate well with the Lower Red Beds, Upper Red Beds and Ludlow Red Beds in south China, respectively^{46,47}. The middle fish-bearing Huixingshao Formation is about 85–350 m thick, and is commonly dominated by greyish green and purplish red (less) argillaceous siltstones, silty mudstones intercalated with fine sandstones. It is conformably overlying the Xiushan Formation and disconformably underlying the Xiaoxi Formation^{43–46}. *T. vividus* was collected from the grey-green argillaceous siltstones of the Huixingshao Formation. The geological age of the Huixingshao Formation can be assigned to the middle–late Telychian of the Llandovery based on gradation of the rocks from the underlying Xiushan Formation, in which the Xiushan fauna is recognized and was assigned to the *Pterospathodus celloni* biozone or *Monoclimacis griestoniensis* biozone of the middle Telychian^{43–45}. All specimens are permanently housed and accessible for examination in the collections of the Institute of Vertebrate Palaeontology and Palaeoanthropology (IVPP), Chinese Academy of Sciences, Beijing.

Specimen preparation

The fossils were prepared mechanically using a vibro tool with a tungsten carbide bit or a needle to remove the surrounding matrix, measured with digital vernier callipers and studied under an Olympus SZ61 zoom stereo microscope.

Imaging and figures

Specimens were optically imaged, using a Nikon D810 camera coupled with a Nikon AF-S Micro Nikkor 60 mm 1:2.8G photo lens and an Olympus SZ61 zoom stereo. The specimens were whitened by coating a non-destructive layer of ammonium chloride sublimate to enhance the details. The details of the pronounced ventrolateral fins in the holotype were examined using Zeiss EVO MA 25 scanning electron microscopy with an energy-dispersive X-ray spectroscopy system at the IVPP. Specimens were uncoated, but surrounded by a circle of electroconductive rubber, and were then mounted on pin stubs using double-sided carbon tape. The vacuum is less than 1.29×10^{-4} mbar, working distance, WD = 17.0 mm, operating voltage, EHT = 3.00 kV, current / probe = 5 pA, signal A = SE1. The image of the three-dimensional restoration was generated using the digital sculpting software Zbrush on the basis of fossil specimens IVPP V26668, V27410 and V27411 (Fig. 2g and Extended Data Fig. 5).

Three-dimensional virtual modelling

Two different digital reconstructions of *Tujiaaspis*, with and without ventrolateral ridges, respectively, were obtained through three-dimensional virtual modelling and using Zbrush. Digital models obtained by this procedure constitute reliable approximations to evaluate function through computational analysis and represent a suitable alternative to those derived from tomographic or surface-based techniques⁴⁸. Digital models were smoothed, repaired and converted into NURBS surface using Geomagic Studio 2012 (www.3dsystems.com) and subsequently converted into STEP format and scaled to life size using Rhinoceros 3D 6.34 (www.rhino3d.com) (Extended Data Fig. 6a).

CFD analyses

Simulations of water flow around the three-dimensional models of *Tujiaaspis* were performed using ANSYS-Fluent 2020 R1 Academic (www.ansys.com). The computational domain consisted of a rectangular prism (1,820 mm in length and 610 mm in both width and height) in which the model was centrally fixed and positioned at 13 different angles of attack (0° to 60°, every 5°) (Extended Data Fig. 6b). The angle of attack is defined here as the angle between the incoming flow and the longitudinal body axis of the fish, thus allowing comparison of biologically analogue positions between the models with and without ventrolateral fins.

An inlet boundary condition with a normal inflow velocity and with a turbulence intensity of 0.05 was defined at the upstream end of the domain and a zero-pressure outlet boundary condition at the downstream end. Slip symmetry boundary conditions were assigned to the sides of the rectangular prism modelling a zero-shear wall, whereas the walls of the model were assigned a no-slip boundary condition, fixing the fluid velocity at zero (Extended Data Fig. 6b).

The domain was meshed with ANSYS-Meshing. Tetrahedral elements were used in the interior and the walls of the rectangular prism. An inflation layer with a maximum of 23 layers of prismatic elements and a growth rate of 1.1 was created at the no-slip boundaries (that is, the walls of the *Tujiaaspis* model) to model the boundary layer region. We added a volume of extra refinement around the wake, consisting of a rectangular prism with a length of 700 mm, height of 200 mm and width of 120 mm. Finally, the domain was converted to a polyhedral mesh (Extended Data Fig. 6c,d). The number and minimum–maximum size of the mesh elements used in the CFD simulations are shown in Supplementary Data 1.

We performed independence tests for mesh size, domain size and refinement volume to ensure that our results were independent of these elements. A solution was considered independent if the converged value for drag and lift forces did not change by more than 1% between a simulation and the next one considering a coarser mesh, bigger domain or refinement volume. The number of inflation layers was also determined by performing mesh sensitivity tests (Supplementary Data 2). We validated the CFD parameters by replicating data in the literature from real water-tank experiments on an ellipsoidal body with similar proportions to *Tujiaaspis* in which turbulence was forced by placing trip strips (Supplementary Data 2).

We simulated three-dimensional, incompressible flow through the domain, with a double precision stationary solver and a second-order discretization method used to compute the steady-state flow. The Reynolds-averaged Navier–Stokes equations were solved using the Spalart–Allmaras model and a pressure-based segregated algorithm. Convergence of the simulations was evaluated on the basis of a stable numerical solution for the integrated values of drag and lift, root-mean-square residual levels of 10^{-4} and a mass flow rate imbalance smaller than 1%. We considered a range of realistic ambient flow velocities (0.3 m s^{-1} , 0.5 m s^{-1} and 1.0 m s^{-1} , with Reynolds numbers of 25,378, 42,296 and 84,593, respectively), in agreement with swimming speed records of similarly sized living fishes⁴⁹.

Plots of pressure (Pa) over the surface of the models and pathlines were used to visualize the results. Drag and lift forces and their coefficients were determined by considering the whole surface of the models as the reference area. The apparent weight of each model was calculated assuming a body density of $1,100 \text{ kg m}^{-3}$, which is based on the highest density records of living taxa⁵⁰ and is a coherent value for galeaspids, according to previous estimations for other stem gnathostomes that considered the distribution and density of the different tissues and internal cavities⁵¹.

To assess the hydrodynamic benefit in lift generation associated with the presence of ventrolateral fins (Extended Data Fig. 7), we tested whether the rate of change of lift force with angle of attack is higher in the model with these structures (before the stall is reached). To do so, we compared the difference in lift force between the models with

and without ventrolateral fins against the angle of attack and assessed the significance of the slope by applying a linear regression analysis. A slope equal to 0 is expected if the rate of change of lift force with angle of attack is equal in both models.

Ancestral-state estimation

We coded 55 taxa (18 extant and 37 extinct) for five discrete characters: (i) paired ventrolateral cephalothoracic dermal skeletal body-wall extensions, absent = 1, present = 2; (ii) paired ventrolateral fins, absent = 1, present = 2; (iii) extent of paired ventrolateral fins, absent = 1, continuous anteroposterior fins = 2, anterior fins only = 3, separate anterior and posterior fins = 4; (iv) pectoral appendicular endoskeleton and girdle, absent = 1, present = 2; (v) pelvic appendicular endoskeleton and girdle, absent = 1, present = 2. Character states were obtained from the literature (table 1 of Supplementary Data 3). Ancestral states were estimated using two phylogenetic hypotheses, either with anaspids as sister to all other ostracoderms + jawed vertebrates (as in ref. ²⁴) or as sister to cyclostomes + conodonts (as in ref. ²⁵). Interrelationships of heterostracans, thelodonts, osteostracans, placoderms and actinopterygians were based on refs. ^{52–56}. First and last occurrence dates for fossil taxa were obtained from the literature (table 2 of Supplementary Data 3). Mean molecular node ages for major chordate clades were obtained from refs. ^{56,57}. Trees were time-scaled using the ‘equal’ method of the function `timePaleoPhy()` from the R package ‘`paleotree`’⁵⁸. Mean molecular node ages for extant clades were used as minimum ages for internal nodes using the `node.mins` argument. In practice, this forces the ages of the internal nodes to be equal to the mean molecular node age. All ancestral states were estimated using the ‘`castor`’ R package⁵⁹. Parsimony ancestral states were estimated using the `hsp_max_parsimony()` function, which permits uncertain tip states. Likelihood ancestral states were estimated using the `asr_mk_model()` function, using the equal rates model. Ancestral states were plotted using the R packages ‘`strap`’⁶⁰ and `phytools`⁶¹. The full results of these analyses are shown in Supplementary Data 4. The R script used for these analyses is available as Supplementary Data 5.

Reporting summary

Further information on research design is available in the Nature Research Reporting Summary linked to this paper.

Data availability

All data analysed in this paper are available in the Article, Extended Data Figs. 1–7 and Supplementary Data 1–5. The nomenclatural acts in this publication have been registered at ZooBank (LSID: urn:lsid:zoobank.org:pub:BD7A6929-33DE-4DDD-ADE2-51A67A489E1B).

Code availability

The R script used for the analyses is available as Supplementary Data 5.

- Rong, J. et al. Silurian integrative stratigraphy and timescale of China. *Sci. China Earth Sci.* **62**, 89–111 (2019).
- Wang, Y. et al. On the late Silurian stratigraphy of the Zhangjiajie area, Hunan province, with a discussion on age of the Xiaoxi Formation. *J. Strat.* **34**, 113–126 (2010).

- Wang, Y. et al. Discovery of the late Silurian Xiaoxi Formation in the Xiushan area, Chongqing city, China, and the revision of the Huixingshao Formation. *J. Strat.* **35**, 113–121 (2011).
- Zhao, W.-J. & Zhu, M. Siluro-Devonian vertebrate biostratigraphy and biogeography of China. *Palaeoworld* **19**, 4–26 (2010).
- Zhao, W. et al. A review of Silurian fishes from north-western Hunan, China and related biostratigraphy. *Acta Geol. Pol.* **68**, 475–486 (2018).
- Rahman, I. A. & Lautenschlager, S. Applications of three-dimensional box modeling to paleontological functional analysis. *Palaeontol. Soc. Pap.* **22**, 119–132 (2016).
- Videler, J. J. *Fish Swimming* (Springer Science & Business Media, 2012).
- Lowndes, A. G. XXXIII.—Density of fishes: some notes on the swimming of fish to be correlated with density, sinking factor and load carried. *Ann. Mag. Nat. Hist.* **8**, 241–256 (1955).
- Botella, H. *Microictiolitos del Devónico Inferior de Nigüella (Cordillera Ibérica); Consideraciones Paleobiológicas e Hidrodinámicas de Condrictios y Agnatos Primitivos* (Univ. València, 2005).
- Randle, E. & Sansom, R. S. Phylogenetic relationships of the ‘higher heterostracans’ (Heterostraci: Pteraspidoformes and Cyathaspididae), extinct jawless vertebrates. *Zool. J. Linn. Soc.* **181**, 910–926 (2017).
- Wilson, M. V. H. & Märss, T. Thelodont phylogeny revisited, with inclusion of key scale-based taxa. *Est. J. Earth Sci.* **58**, 297–310 (2009).
- Sansom, R. S. Phylogeny, classification and character polarity of the Osteostraci (Vertebrata). *J. Syst. Palaeontol.* **7**, 95–115 (2009).
- Lu, J., Giles, S., Friedman, M., den Blaauwen, J. L. & Zhu, M. The oldest actinopterygian highlights the cryptic early history of the hyperdiverse ray-finned fishes. *Curr. Biol.* **26**, 1602–1608 (2016).
- Dornburg, A., Townsend, J. P., Friedman, M. & Near, T. J. Phylogenetic informativeness reconciles ray-finned fish molecular divergence times. *BMC Evol. Biol.* **14**, 169 (2014).
- Delsuc, F. et al. A phylogenomic framework and timescale for comparative studies of tunicates. *BMC Biol.* **16**, 39 (2018).
- Bapst, D. W. `paleotree`: an R package for paleontological and phylogenetic analyses of evolution. *Methods Ecol. Evol.* **3**, 803–807 (2012).
- Louca, S. & Doebeli, M. Efficient comparative phylogenetics on large trees. *Bioinformatics* **34**, 1053–1055 (2018).
- Bell, M. A. & Lloyd, G. T. `strap`: an R package for plotting phylogenies against stratigraphy and assessing their stratigraphic congruence. *Paleontology* **58**, 379–389 (2015).
- Revell, L. J. `phytools`: an R package for phylogenetic comparative biology (and other things). *Methods Ecol. Evol.* **3**, 217–223 (2012).

Acknowledgements We thank R. Freitas for helpful discussion on mechanisms of fin development, R. Zhao, X. Shan, X. Lin, L. Peng, L. Jia, Q. Wang, Q. Wen, Q. Rao, Y. Zhao, Q. Xue, Z. Xian, X. Meng, Y. Luo, Y. Yan, H. Wang, Q. Deng, J. Xiong, C. H. Xiong, C. Y. Xiong, J. Zhang, Y. Chen, Z. Zhou and L. Nie for the fieldwork assistance, J. Xiong for the specimen preparation, J. Rong and Y. Wang for discussion on stratigraphy, A. Shi for drawing the interpretive illustrations, Q. Zheng for drawing the artistic life restoration, D. Yang for generating the 3D reconstruction, L. Peng and L. Jia for photographing the fossil and X. Jin for scanning electron microscopy imaging. This work was supported by the National Natural Science Foundation of China (42130209, 41972006, 42072026), the Key Research Program of Frontier Sciences, CAS (QZDB-SSW-DQC040), the Strategic Priority Research Program of CAS (XDA19050102, XDB26000000), the National Program for support of Top-notch Young Professionals and Mee-mann Chang Academician Workstation of Yunnan province. P.C.J.D. was funded by the Natural Environment Research Council (NE/G016623/1, NE/P013678/1), the Biotechnology and Biological Sciences Research Council (BB/T012773/1) and the Leverhulme Trust (RF-2022-167). H.G.F. was funded by the European Commission through a Marie Skłodowska-Curie Research Fellowship (H2020-MSCA-IF-2018-839636). J.N.K. was funded by ERC grant no. 788203 (INNOVATION).

Author contributions M.Z. and P.C.J.D. conceived the project. M.Z., J.W., Z.G. and Q.L. conducted the fieldwork, fossil preparation and fossil curation. Z.G., P.C.J.D., M.Z. and H.G.F. contributed to fossil interpretation and wrote the manuscript. H.G.F. and P.C.J.D. conducted computational fluid-dynamics analyses. J.N.K. undertook the ancestral-state reconstruction analyses. All authors edited and approved the manuscript.

Competing interests The authors declare no competing interests.

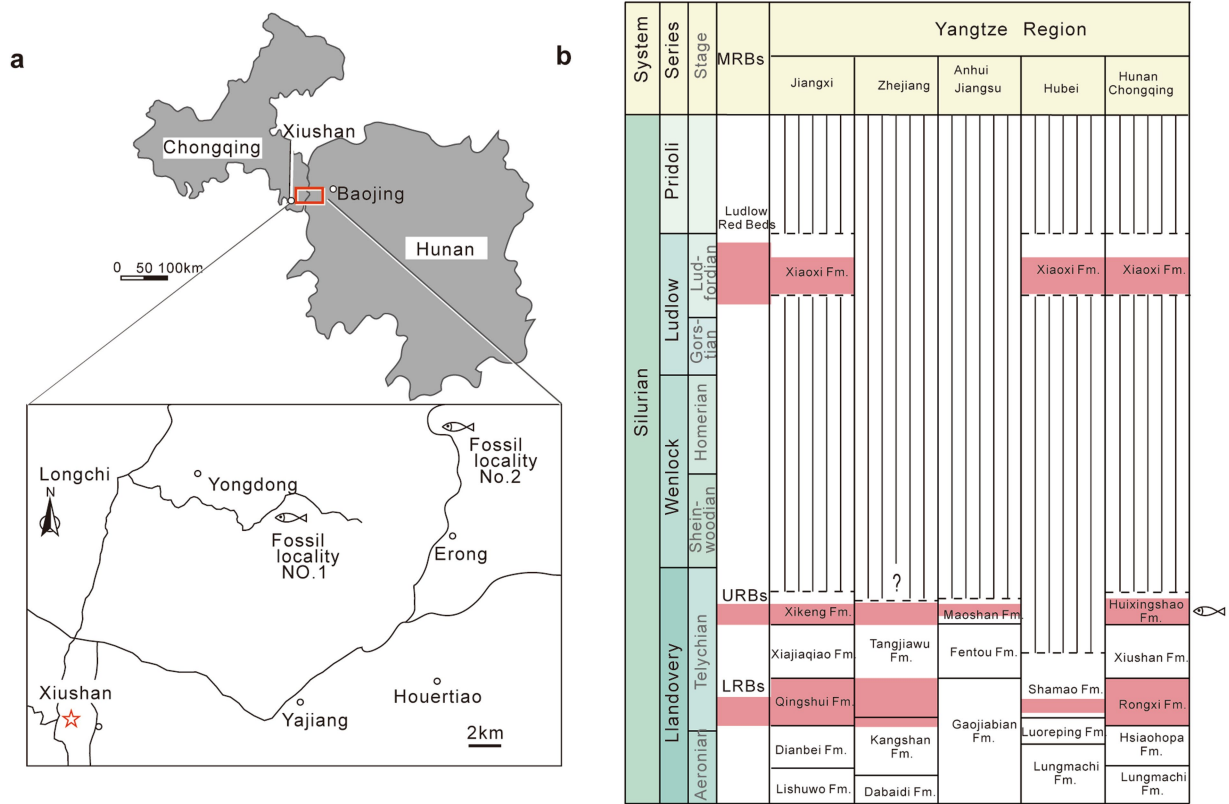
Additional information

Supplementary information The online version contains supplementary material available at <https://doi.org/10.1038/s41586-022-04897-6>.

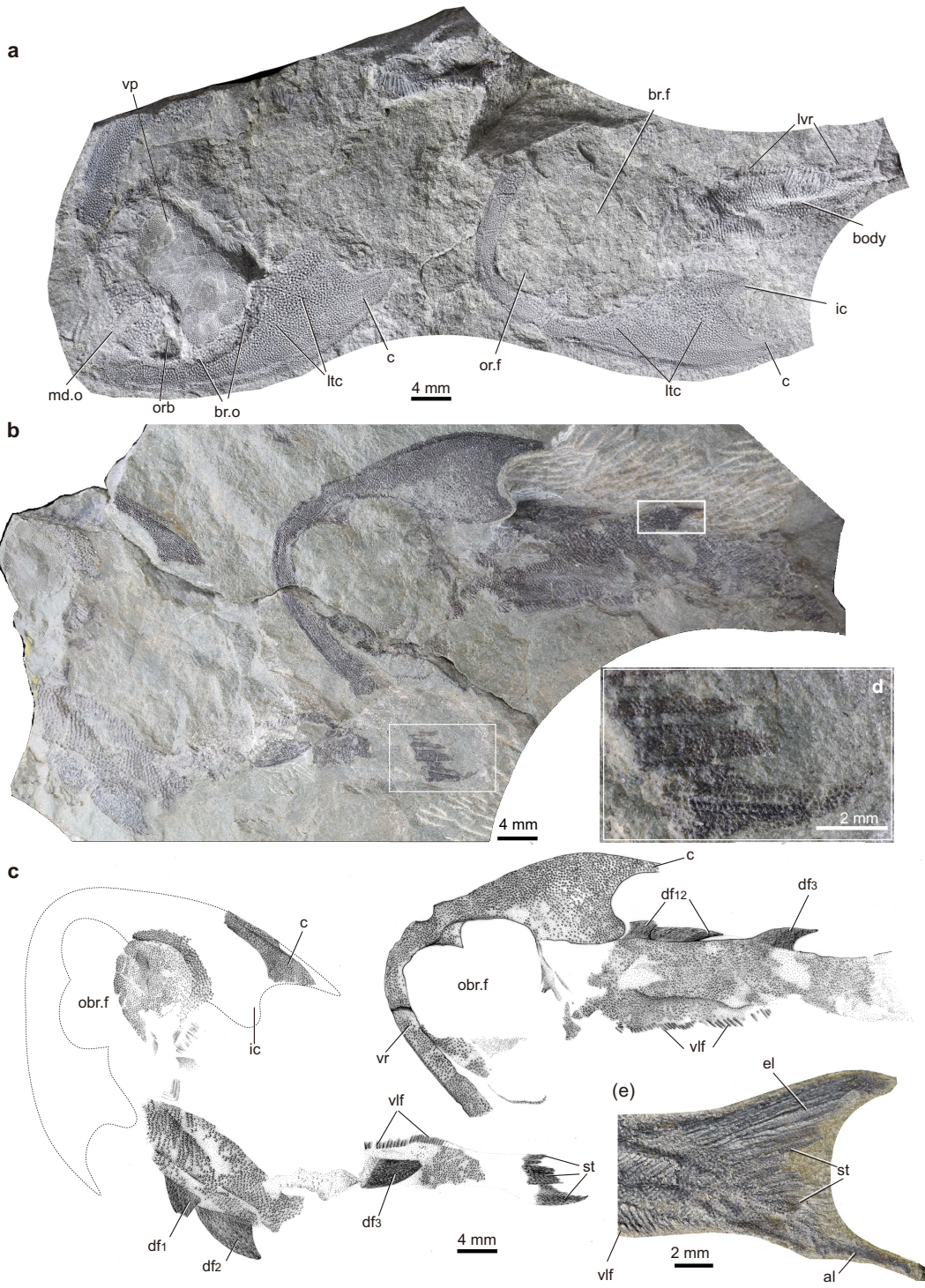
Correspondence and requests for materials should be addressed to Philip C. J. Donoghue or Min Zhu.

Peer review information Nature thanks John Dabiri, Matt Friedman and the other, anonymous, reviewer(s) for their contribution to the peer review of this work.

Reprints and permissions information is available at <http://www.nature.com/reprints>.

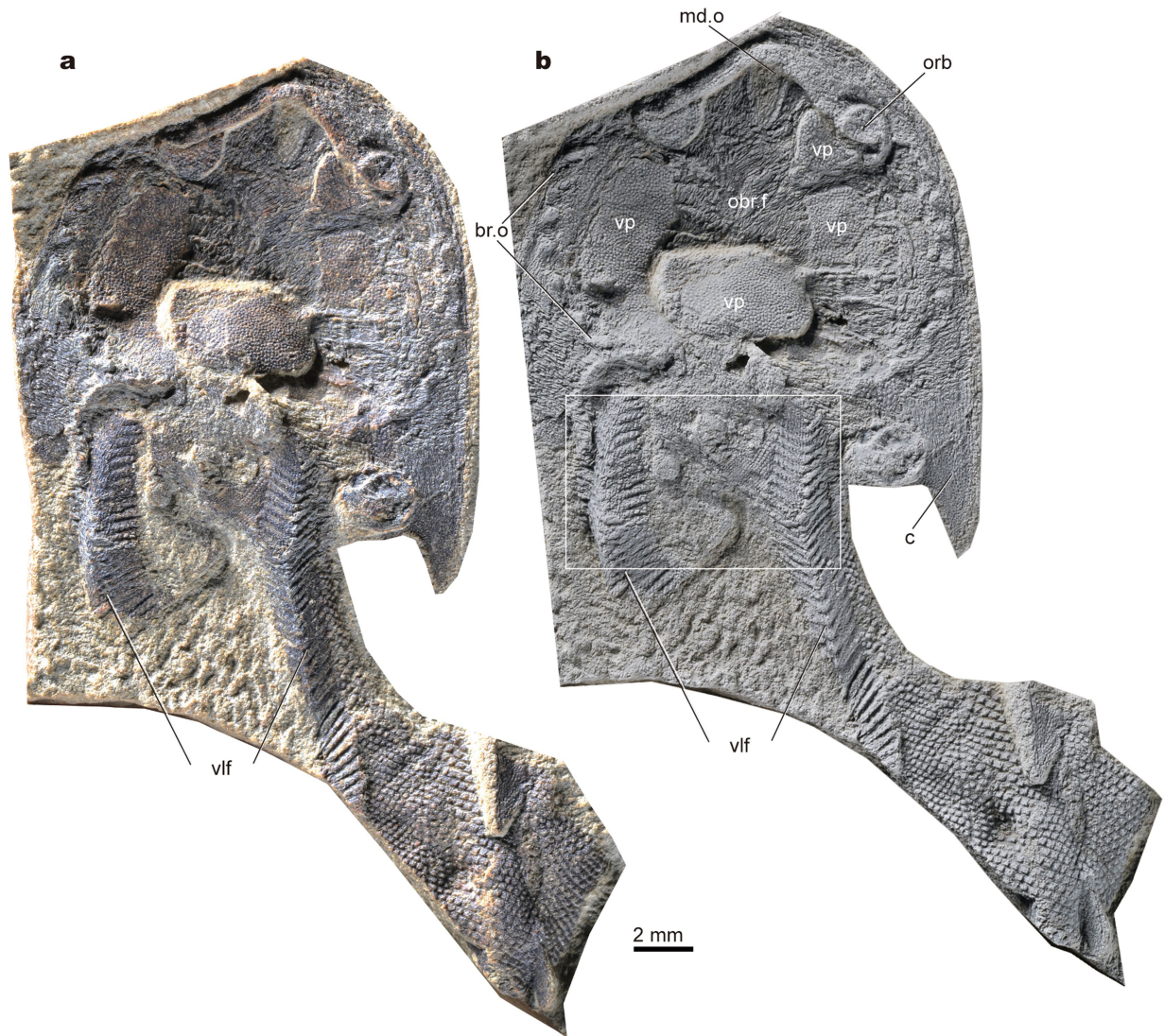


Extended Data Fig. 1 | Geological setting of *Tujaaspis vividus*. **a**, Maps of the two fossil localities in Xiangxi and Xiushan Tuja and Miao Autonomous Prefecture (County). **b**, Horizon of the fish-bearing Huixingshao Formation.



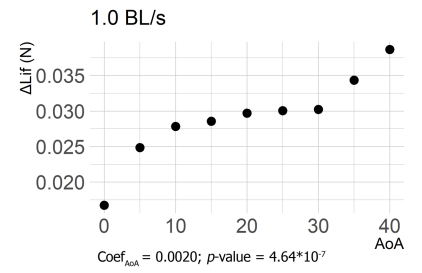
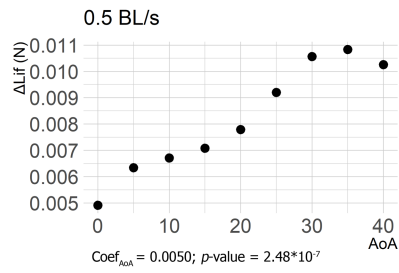
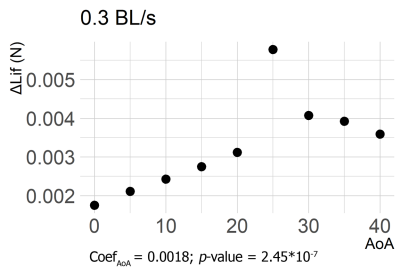
Extended Data Fig. 2 | The postcranial anatomy of *Tujiaaspis vividus*. uncoated counterpart (b) with an interpretative drawing (c), the paratype, IVPP V27410 (right, in dorsal view) and V27411 (left, in ventral view). d, Close-up

of the tail magnified from the box region of (b), in lateral view. e, Close-up of the tail of the holotype, IVPP V26668, in lateral view. Abbreviations as in Figs. 1, 2.

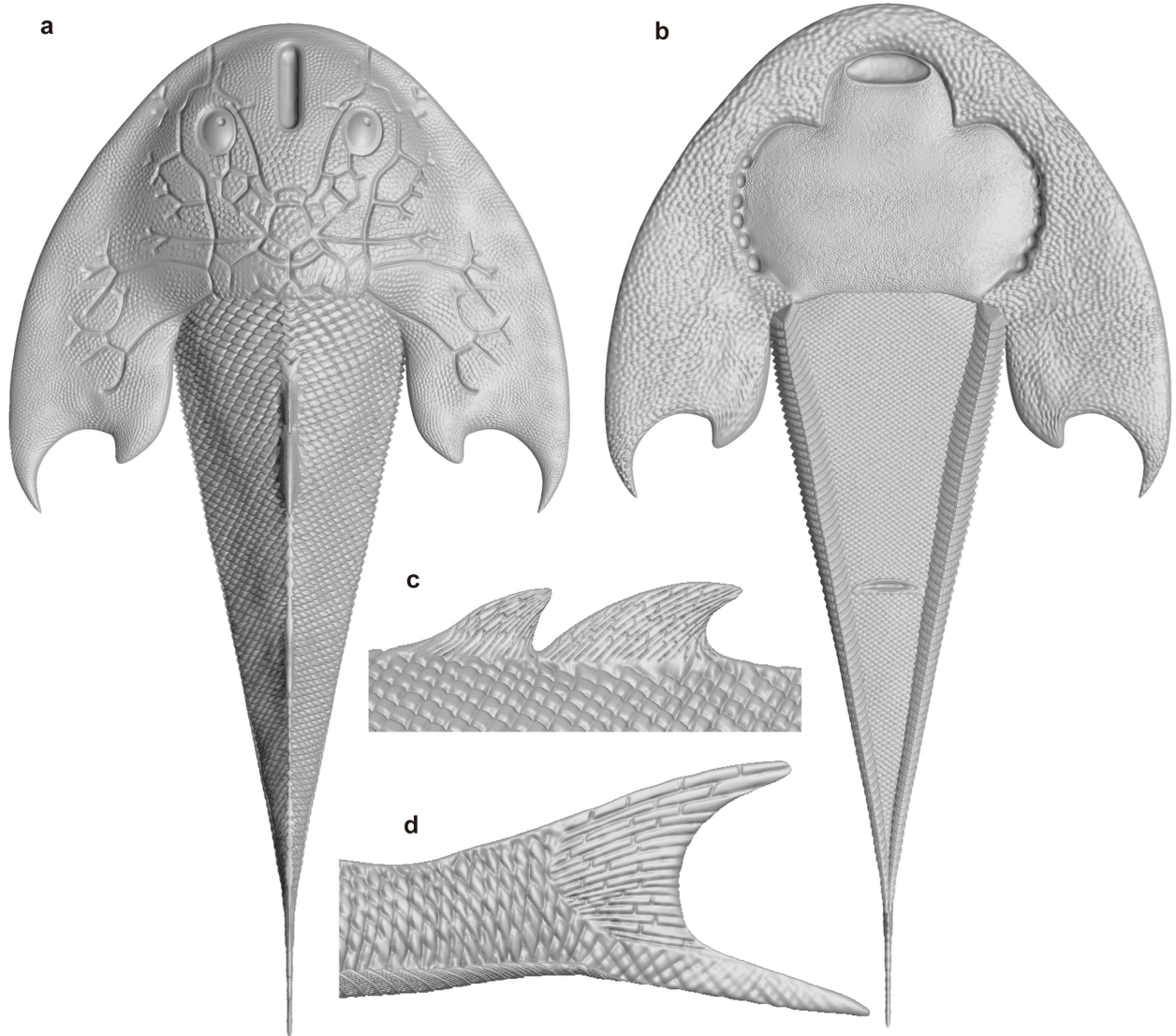


Extended Data Fig. 3 | The postcranial anatomy of another new form of *Eugaleaspidiformes* from the same locality and horizon with the holotype of *Tujiaaspis vividus*. a, b. Photographs of specimen IVPP V26669 uncoated (a)

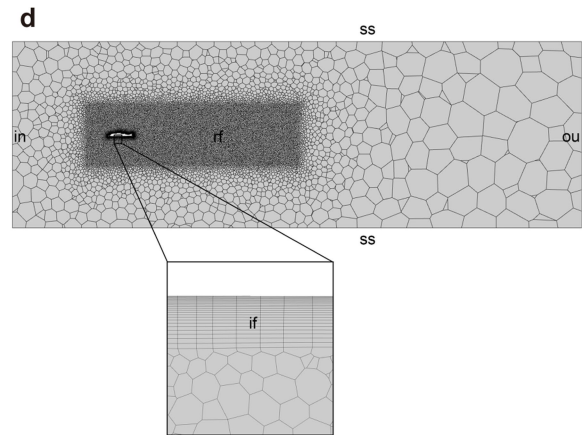
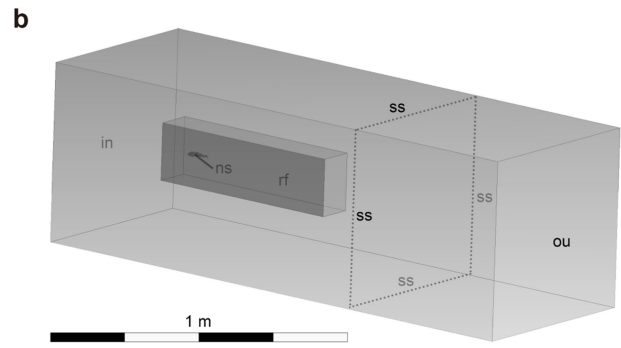
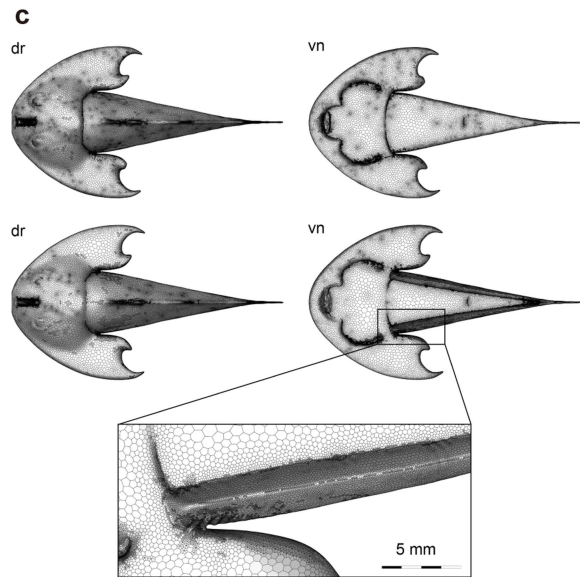
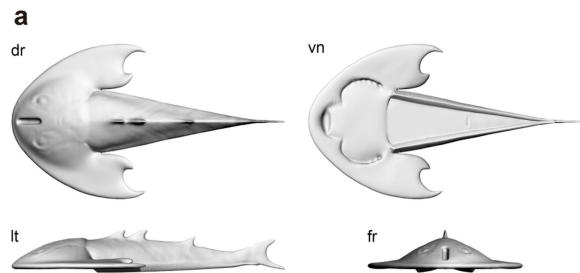
and coated (b) by a layer of ammonium chloride sublimate, respectively, in ventral view. Abbreviations as in Figs. 1, 2.



Extended Data Fig. 4 | Difference in lift force (N) between the models with and without ventrolateral fins (Δ Lift) against the angle of attack (AoA). Linear regression coefficient and significance of the slope is showed.

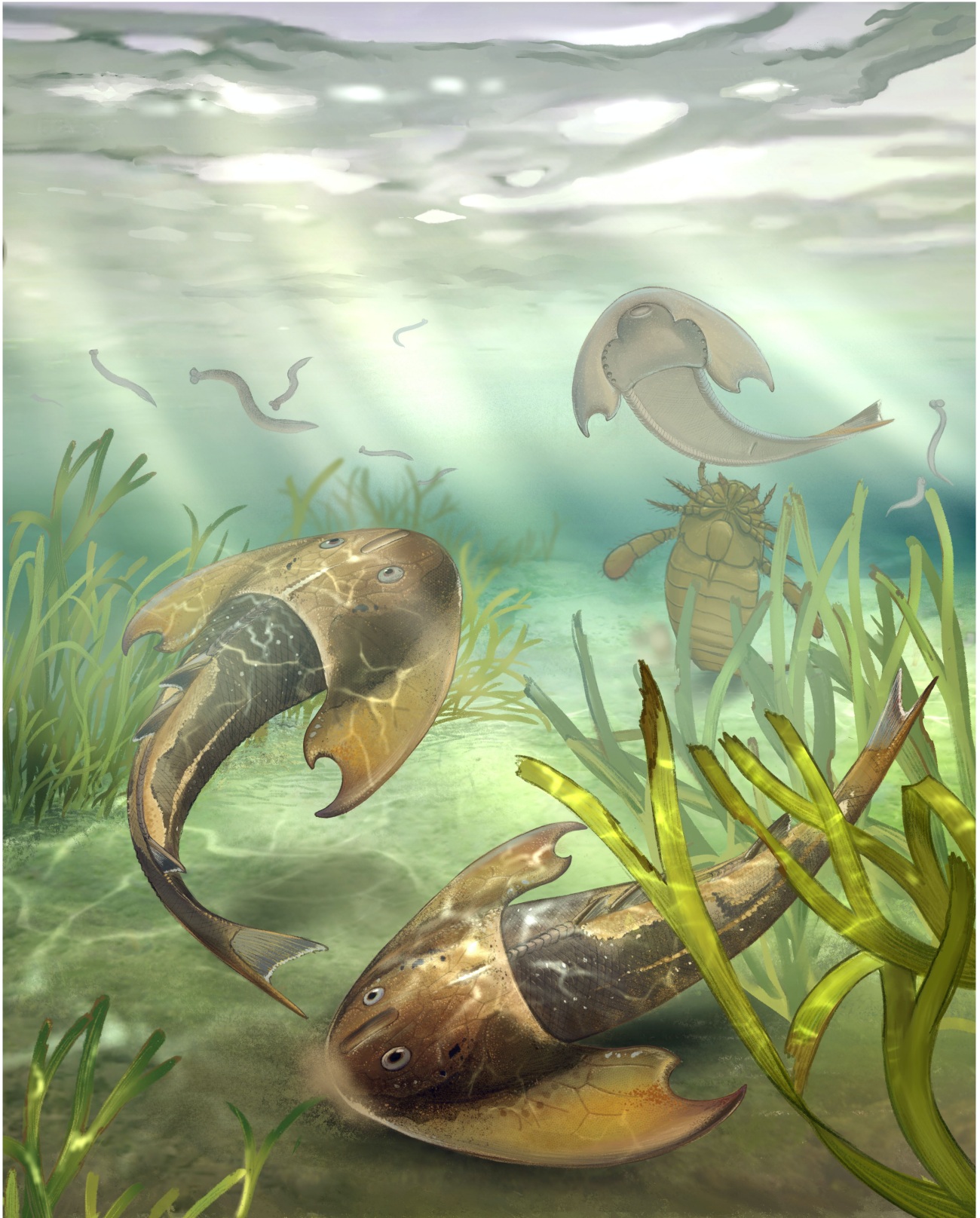


Extended Data Fig. 5 | 3D virtual restoration of *Tujaaspis vividus*. **a**, In dorsal view. **b**, In ventral view. **c**, Close-up of the anterior two dorsal fins. **d**, Close-up of the tail, (**c,d**), in lateral view.



Extended Data Fig. 6 | Computed Fluid Dynamics analysis of *Tujaaspis vividus*. **a**, 3D model including ventrolateral ridges in dorsal (dr), ventral (vn), lateral (lt) and frontal (fr) views. **b**, **c**, **d**, Computational domain (**b**), mesh overlying the models without (upper) and with (lower) ventrolateral fins in

dorsal (dr) and ventral (vn) views, and general mesh (**c**) employed in the CFD analysis noting the different boundary conditions (in, inlet; ou, outlet; ns, non-slip; ss, slip symmetry), refinement volume (rf) and inflation layers (if).



Extended Data Fig. 7 | The artistic life restoration of *Tujaaspis vividus* (Picture credit Qiuyang Zheng). The ventral side of the body in *Tujaaspis vividus* manifests a pair of continuous pectoral-pelvic lateral fins which our

Computed Fluid Dynamic experiments demonstrate passively generate lift to escape from predators such as sea scorpions to escape from predators such as sea scorpions.

Reporting Summary

Nature Research wishes to improve the reproducibility of the work that we publish. This form provides structure for consistency and transparency in reporting. For further information on Nature Research policies, see [Authors & Referees](#) and the [Editorial Policy Checklist](#).

Statistics

For all statistical analyses, confirm that the following items are present in the figure legend, table legend, main text, or Methods section.

n/a Confirmed

- The exact sample size (n) for each experimental group/condition, given as a discrete number and unit of measurement
- A statement on whether measurements were taken from distinct samples or whether the same sample was measured repeatedly
- The statistical test(s) used AND whether they are one- or two-sided
Only common tests should be described solely by name; describe more complex techniques in the Methods section.
- A description of all covariates tested
- A description of any assumptions or corrections, such as tests of normality and adjustment for multiple comparisons
- A full description of the statistical parameters including central tendency (e.g. means) or other basic estimates (e.g. regression coefficient) AND variation (e.g. standard deviation) or associated estimates of uncertainty (e.g. confidence intervals)
- For null hypothesis testing, the test statistic (e.g. F , t , r) with confidence intervals, effect sizes, degrees of freedom and P value noted
Give P values as exact values whenever suitable.
- For Bayesian analysis, information on the choice of priors and Markov chain Monte Carlo settings
- For hierarchical and complex designs, identification of the appropriate level for tests and full reporting of outcomes
- Estimates of effect sizes (e.g. Cohen's d , Pearson's r), indicating how they were calculated

Our web collection on [statistics for biologists](#) contains articles on many of the points above.

Software and code

Policy information about [availability of computer code](#)

Data collection Photographs of the fossils were taken using Nikon D850 Full Frame Digital SLR Camera, the Broncolor Scope D50 light dome containing 48 LEDs, and the Zeiss EVO MA 25 scanning electron microscopy(SEM) in IVPP with an energy-dispersive X-ray spectroscopy.

Data analysis The picture of 3D restoration is generated by the digital sculpting software Zbrush. Digital models were repaired and converted into NURBS surface using Geomagic Studio 2012 (www.3dsystems.com) and subsequently converted into STEP format and scaled to life size using Rhinoceros 3D 6.34 (www.rhino3d.com). Computational fluid dynamics analyses were performed using ANSYS-Fluent 2020 R1 Academic. Ancestral state reconstructions were conducted in R programming language (www.r-project.org) using the packages 'paleotree' (Bapst 2012), 'castor' (Louca & Doebeli 2018), 'strap' (Bell & Lloyd 2015) and 'phytools' (Revell 2012). The custom script for our ancestral state reconstructions is included in our supplementary material.

For manuscripts utilizing custom algorithms or software that are central to the research but not yet described in published literature, software must be made available to editors/reviewers. We strongly encourage code deposition in a community repository (e.g. GitHub). See the Nature Research [guidelines for submitting code & software](#) for further information.

Data

Policy information about [availability of data](#)

All manuscripts must include a [data availability statement](#). This statement should provide the following information, where applicable:

- Accession codes, unique identifiers, or web links for publicly available datasets
- A list of figures that have associated raw data
- A description of any restrictions on data availability

The authors declare that all data, including the photographs (Figures 1, 2, and Extended Data Figures 2–4), computational fluid dynamics analysis files (see Supplementary data) that support the findings of this research are included. All the specimens (IVPP V26668, V26669, V27410, V27411) described in this study are archived and available on request from the Institute of Vertebrate Paleontology and Paleoanthropology, Chinese Academy of Sciences, Beijing, China.

Field-specific reporting

Please select the one below that is the best fit for your research. If you are not sure, read the appropriate sections before making your selection.

Life sciences Behavioural & social sciences Ecological, evolutionary & environmental sciences

For a reference copy of the document with all sections, see [nature.com/documents/nr-reporting-summary-flat.pdf](https://www.nature.com/documents/nr-reporting-summary-flat.pdf)

Ecological, evolutionary & environmental sciences study design

All studies must disclose on these points even when the disclosure is negative.

Study description	In this study, which stands as one of a batch of the papers on the early Silurian Chongqing Lagerstätte, we report several superbly preserved jawless galeaspid specimens, which, for the first time, reveal the details of the postcranial anatomy in Galeaspida that is sister to osteostracans and jawed vertebrates.
Research sample	Investigated materials were collected from a horizon of the Huixingshao Formation. Sample size comprises all available material attributed to the new taxon.
Sampling strategy	Standard bulk sampling protocols for vertebrate fossils were followed in the collection and extraction of studied specimens. Selection of a holotype and referred specimens was dictated by specimen completeness and whether the specimen yields further morphological information than other specimens.
Data collection	Sediment samples from a horizon of the Huixingshao Formation were collected by the authors during field trips to the site from 2020-2021. Data collection involving observation and recording of specimen features employing light microscopy, and scanning electron microscopy was performed from November 2020 to August 2021.
Timing and spatial scale	N/A
Data exclusions	No data is excluded. We examined all the available specimens attributed to the <i>Tujiaaspis</i> described.
Reproducibility	The results of the analyses in this study can be reproduced and verified by re-analyzing the given data set.
Randomization	N/A. Not applicable to the study as it does not have an experimental component.
Blinding	N/A. The study is not subject to selection bias and thus blinding is not applicable to the investigation of this previously undescribed fossil material.
Did the study involve field work?	<input checked="" type="checkbox"/> Yes <input type="checkbox"/> No

Field work, collection and transport

Field conditions	The weather of the field site varied during the field season. The fossils were collected from outcrops naturally exposed, mostly on the roadside. The excavation was conducted manually.
Location	The section through the Huixingshao Formation at Yongdong, Xiushan County, Chongqing, and Kapeng, Hunan.
Access and import/export	This is part of a project supported by the Chinese Academy of Sciences and the National Natural Science Foundation of China. The access to the field region follows the national laws.
Disturbance	There is no disturbance in the field region. After collection, the outcrops were restored to the original status by the field team.

Reporting for specific materials, systems and methods

We require information from authors about some types of materials, experimental systems and methods used in many studies. Here, indicate whether each material, system or method listed is relevant to your study. If you are not sure if a list item applies to your research, read the appropriate section before selecting a response.

Materials & experimental systems

- n/a Involved in the study
- Antibodies
- Eukaryotic cell lines
- Palaeontology
- Animals and other organisms
- Human research participants
- Clinical data

Methods

- n/a Involved in the study
- ChIP-seq
- Flow cytometry
- MRI-based neuroimaging

Palaeontology

- Specimen provenance The specimens, which were collected and processed by the authors, belong to Institute of Vertebrate Paleontology and Paleoanthropology, Chinese Academy of Sciences.
- Specimen deposition The specimens are housed in Institute of Vertebrate Paleontology and Paleoanthropology, Chinese Academy of Sciences. They are available on request.
- Dating methods The Silurian strata in the Xiushan County of Chongqing and the neighboring Guizhou and Hunan provinces have been extensively studied. The dating of the fossil is based on the well-established stratigraphic sequence.
- Tick this box to confirm that the raw and calibrated dates are available in the paper or in Supplementary Information.